ADVANCED OPTICAL MATERIALS
www.advopticalmat.de

Organic Source-Gated Phototransistors with > 10^4 Photo-To-Dark Current Ratio in the Visible Range at Zero Gate-Source Bias

Eva Bestelink, Ute Zschieschang, Leslie Askew, Hagen Klauk, and Radu A. Sporea**

With growing interest in organic phototransistors, as not only sensors but also neuromorphic computing elements, the vast majority of research investigates structures comprising Ohmic source/drain contacts. Here, it is shown how source-gated transistors (SGTs), in which a source contact barrier dominates electrical characteristics, can be implemented as phototransistors. Organic photo-SGTs (OPSGTs) based on vacuum-processed small-molecule dinaphtho[2,3-b:2′,3′-f]thieno[3,2-]thiophene (DNTT) demonstrate low saturation voltage, exceptional tolerance to channel length variation, and photo-to-dark current ratio (PDCR) peaks over 10^6 for 819 µW broad spectrum incident light power. At zero gate-source voltage, the PDCR reaches 10^4, showing promise for simple sensor circuit implementation in medical and wellbeing applications.

1. Introduction

Organic photodetectors, and more specifically, organic phototransistors (OPTs), have been a prominent area of research for quite some time.[1] Currently, there is an escalating interest in detecting a wide array of optical signals with applications in various domains, such as sensor technology, medical imaging, nocturnal visualization, optical isolation, phase modulation, data storage memory, and neuromorphic computational systems.[1–6] Typically, the types of device architectures used in OPT applications have been implemented based on the traditional field-effect transistor (FET) operation, whereby drain current is modulated by the resistance of the channel. Photogenerated current, however, depends on two mechanisms[6]: charge trapping of light-induced minority carriers, which shifts the threshold voltage V_{th}; and accumulation of majority carriers, which increases the on-current. Yet, even though the operating principles of OPTs do not necessarily rely on the field effect, OPT researchers generally aim to fabricate devices with Ohmic contacts.[6,7] Thus, contact resistance is widely regarded as a nuisance for thin-film transistors (TFTs) and their counterparts, OPTs, however, there have been exceptions.[3]

Although the prevailing tendency in transistor design is to avoid energy barriers, an emerging TFT architecture, the source-gated transistor (SGT)[8] has been comparatively less investigated. SGTs are a type of TFT that specifically rely on energy barriers at the source contact (**Figure 1**a,b) for their unique operation.[9,10] While there is growing interest in the device,[11] since its invention by Shannon and Gerstner 20 years ago,[8] to our knowledge there has been no study into SGT-based OPTs.

Here, we present small-molecule dinaphtho[2,3-b:2′,3′-f]thieno[3,2-]thiophene (DNTT, Figure 1c)[12] organic SGTs (OSGTs, Figure 1d)[13,14] and their behavior when exposed to an optical stimulus in the visible range. DNTT OPTs have been implemented in gesture recognition[7] and are capable of low light detection in the pW cm^{-2} range,[6] with a sensitivity to ultraviolet (UV) and blue light (peak wavelength λ = 450 nm).[6,7,15] Yet, they have not been explored in SGT architectures.

As a first step toward development of new types of OPSGTs as sensors, we first discuss device operation of SGTs versus TFTs, and explore some of the benefits in light of V_{th} variation and temperature dependence, before considering optical behavior when exposed to a 2650 K "warm white" cold light illuminator (Figure 1e,f).

As the SGT is a type of device architecture and is material agnostic, the principles presented here would be applicable to many material systems and other contact-controlled devices,[16] as long as a reliable energy barrier can be engineered at the source contact. By implementing transistors with three different contact metals (Au, Cu, and Ni), we highlight the importance of contact engineering to the electrical and optoelectronic properties of such thin-film transistors.

Here, we show the interesting operation that can be produced by varying the contact metal. Based on this initial understanding

E. Bestelink, L. Askew, R. A. Sporea
Advanced Technology Institute
School of Computer Science and Electronic Engineering
University of Surrey
Guildford GU2 7XH, UK
E-mail: r.a.sporea@surrey.ac.uk

U. Zschieschang, H. Klauk
Max Planck Institute for Solid State Research
70569 Stuttgart, Germany
E-mail: h.klauk@fkf.mpg.de

The ORCID identification number(s) for the author(s) of this article can be found under https://doi.org/10.1002/adom.202301931

DOI: 10.1002/adom.202301931

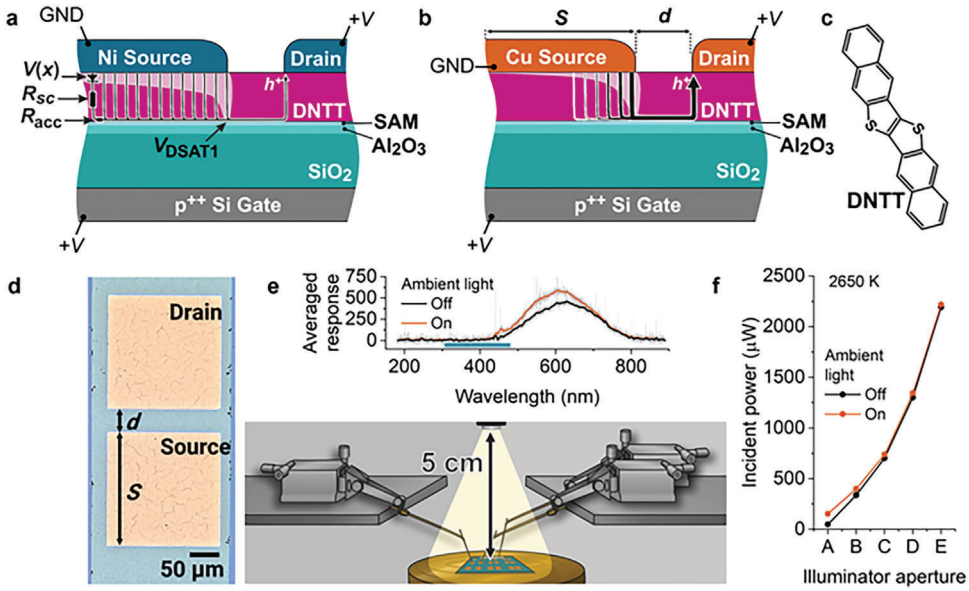

Figure 1. Cross-section schematics of source-gated transistors (SGTs) with a) Ni and b) Cu top contacts. Pinch-off at the source occurs at V_{DSAT1} and the charge injected along the source-gate overlap (S) region depends on the vertical resistance of the semiconductor R_{sc} and horizontal resistance of the accumulation layer R_{acc}. Higher energy barriers at the source lead to smaller potential drops $V(x)$ along S, hence more of S contributes to charge injection in the Ni devices. The lower barrier in Cu results in increased drain current and less $V(x)$ to facilitate charge injection from farther regions of S. c) Dinaphtho[2,3-b:2′,3′-f]thieno[3,2-]thiophene (DNTT). d) Photomicrograph of the top view of fabricated Ni SGTs, showing parameters S and source-drain gap d. e) Averaged spectral response of the optical source and setup for incident light experiments. The teal region indicates the spectral range of maximum absorption of DNTT. f) Incident power with doubling of illuminator aperture area. The contribution of ambient room light is not significant at higher aperture settings.

may come future developments, which take advantage of both architecture and wavelength-specific materials for optoelectronic applications with low implementation cost.

First, we report transistor characteristics for the three different contact metals (see Experimental Section for details on device fabrication and characterization), explaining the evolution of the operation from the more well-known FET-type TFTs and the progression toward SGT behavior by varying the contact metal. Second, we show some of the benefits of fabricated OSGTs in accordance with well-established operating principles, including their unique temperature dependence as DNTT OSGTs, which has been previously observed in a different contact metal.[14] Finally, we operate the structures as OPSGTs under illumination in the visible range.

2. Results and Discussion

2.1. Source-Gated Transistor Operating Principles

As indicted by their name, source-gated transistors rely on the source contact to control charge injection, whereby the source-gate overlap modulates the drain current.[8–10,17] Hence, they are contact-controlled devices as opposed to conventional thin-film FETs, which are channel-controlled.

The output characteristics of an Ohmic-contact TFT (**Figure 2**a), with Au electrodes, are typical of the expected saturation behavior based on channel-controlled operation of field-effect transistors.[18] For a change of saturation voltage V_{DSAT} with gate-source voltage V_{GS}, we would expect a unity value ($dV_{DSAT}/dV_{GS} = 1$), as drain pinch-off occurs, in the first order, at $V_{DSAT2} = V_{GS}-V_{th}$ (For clarity, V_{DSAT} can refer to early source-side pinch-off at V_{DSAT1} or drain-side pinch-off at V_{DSAT2}, depending on the context). Similarly, the output characteristics of the device with Cu contacts demonstrate the same $dV_{DSAT}/dV_{GS} = 1$ behavior, yet there are noticeable differences. The slope of the linear regime is comparatively steeper and there is negative differential resistance (NDR) after saturation.[14] The Ni-contact devices, however, demonstrate behavior that is typical of SGTs, with low saturation voltages. The ideal flat saturation that leads to extremely high intrinsic gain[19,20] in these devices is absent, due to the NDR. In accordance with previous studies,[21,22] NDR appears in source-gated transistors in various technologies[14,23,24] and authors have indicated that this is likely due to trap formation at the interfaces.[14] This phenomenon may be more pronounced in SGTs than in TFTs due to the reduced drain current. Even though non-ideal, recent complementary InGaZnO and DNTT SGT inverters[23] were capable of achieving high gain of 368 VV^{-1}. Naturally, improvements in fabrication processes would lead to even higher levels of small-signal gain, But the NDR was not detrimental to inverter performance.

The $dV_{DSAT}/dV_{GS} = 0.28$ in the SGT, which is close to the saturation coefficient $\gamma = 0.26$,[13,14] has been calculated using the dielectric model:

$$\gamma = \frac{C_i}{C_i + C_s} \quad (1)$$

where C_i and C_s are the series-specific capacitances of the gate insulator and depleted semiconductor, respectively. Thus, the thicknesses and permittivities of these layers can be chosen to design

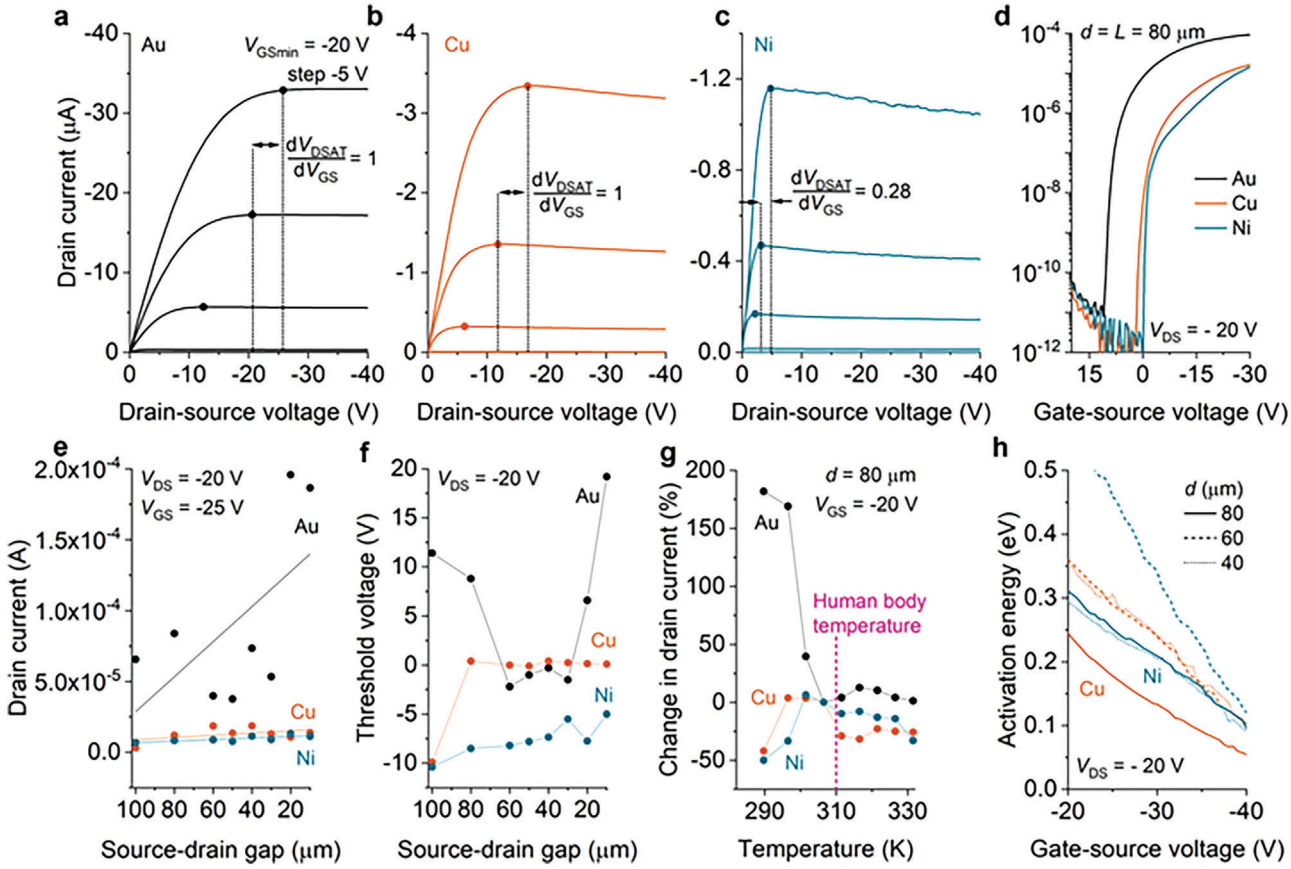

Figure 2. Output characteristics of a) Au, b) Cu, and c) Ni contact transistors, demonstrating field-effect transistor (FET) saturation at $dV_{DSAT}/dV_{GS} = 1$ for Au and Cu devices, and early SGT saturation at $dV_{DSAT}/dV_{GS} = 0.28$. d) Transfer characteristics for transistors with different contact metals. e) Drain current does not vary greatly with source-drain gap d (channel length L in Au FET), demonstrating that Cu contact devices are likely behaving as SGTs with poor saturation, rather than FETs. f) Threshold voltage V_{th} variation shows remarkable stability of Cu contact devices, which is an additional hallmark of SGT operation. g) DNTT OSGTs show low variations of drain current with temperature in a range of interest for on-skin applications. h) Activation energy of drain current extracted from transfer characteristics taken at different temperatures, showing significant bias dependence, in particular for the Ni-contact transistor with $d = 60$ μm.

a specific early drain-voltage saturation V_{DSAT1} point for a given V_{GS}, where $V_{DSAT1} = \gamma\,(V_{DSAT2}) + K$. The constant K represents the small potential required to deplete the active/insulator interface from charge carriers at $V_{GS} = V_{th}$.[25] From this equation, we note that in SGTs, the channel will pinch-off at the source first, due to the drain voltage reverse-biasing the rectifying contact at the source until it fully depletes the active layer under the source edge (Figure 1a), and, with further drain-voltage increase, the channel will pinch-off at the drain side.[26] The drain current in SGTs is then produced in the source-gate overlap region S and is controlled by the potential in the source pinch-off region, namely V_{DSAT1}. In the S region, a proportion $V(x)$ of V_{DSAT1} is dropped along each point of the resistive diode network that forms between the vertical resistance of the semiconductor R_{sc} and lateral resistance in the accumulation layer R_{acc} (Figure 1a).[9,10] This is called Mode II current, which is generally much larger than the thermionic-field emission current (Mode I) at the source edge.[9]

The trade-off for low-voltage saturation and high output impedance comes at the price of reduced transconductance g_m (Figure 2d).[27] In disordered semiconductors, chemical and physical interactions between the contact metal and the semiconductor will often result in rectification properties, which are not directly correlated to the work-function difference.[28] The odd one out, it would seem, is the case of the device with Cu contacts. It does not have the benefits of low-voltage saturation or high g_m that the devices with Ni or Au contacts, respectively, have to offer, nor is it easy to determine whether it operates as an SGT or FET on first inspection.[13]

2.2. Effects of Channel Geometry and Temperature

To explore the behavior of the Cu-contact device, we look at other features of SGT behavior. As previously mentioned, in SGTs, a large extent of the source area participates in charge injection, which is not the case for Ohmic-contact transistors. One method to assess for contact-controlled operation would be to compare the current–voltage characteristics of transistors with different S.[17] However, all fabricated SGTs have the same S, so we continue by testing the next feature, specifically the independence of the SGT drain current on the source-drain gap (denoted d if referring to the electrode separation, and L when identifying the

channel length, to account for the floating source induced by the pinch-off region at the source) (Figure 2e). In principle, and even without interfacial treatment, Au contacts to DNTT should demonstrate an inversely proportional relationship between saturated drain current and L.[18] We have reported such operation in a previous study,[14] but this is not immediately apparent in this batch of devices. The Cu-contact and Ni-contact devices show independence, or a very low dependence, on d, respectively. As such, the Cu-contact devices are likely to be Schottky-contact SGTs, but with higher charge injection, which would require additional V_{DS} to fully pinch-off the source.[13] Increased charge injection also means that more V_{DSAT1} is dropped across the resistance of the S region nearest to the source edge (Figure 1b), leaving much less $V(x)$ to facilitate injection along further points of S. This occurrence, linked to the effective charge-injection area,[29] manifests itself as a saturation of the drain current with S, at a value S_{SAT}.[17]

While the Cu-contact transistor might not offer the best performance in terms of g_m or V_{DSAT1}, it has a highly stable V_{th} (Figure 2f), which is around zero. This is another hallmark of SGT operation. This is due to the quasi-Fermi level of the SGT remaining in the middle of the bandgap during operation, unlike that of FETs, which shifts toward the conduction band (in amorphous Si SGTs).[30] Thus, any defects or trap states formed, do not translate to shifts in V_{th} in SGTs. It is likely the same principle applies here, save for the quasi-Fermi level moving toward the lowest unoccupied molecular orbital (LUMO) of DNTT in Au contact devices.

The temperature stability of these devices is also exceptional for transistors with Schottky contacts (Figure 2g). This is due to the interplay between the degrading mobility of the DNTT offsetting the increased injection from thermionic-field injection over the Schottky barrier.[14] Here, there is a decrease of ≈30% in both Ni-contact and Cu-contact OSGTs, which is similar to previously reported DNTT OSGTs with TiAu contacts.[14] For comparison, in polycrystalline Si Schottky-barrier SGTs, the current would increase by ≈300%.[14,31] As the human-body temperature is ≈310 K, the DNTT OSGTs would be suitable for use in smart tattoos or wearables for indoor healthcare monitoring, with relatively low variation in their static electrical characteristics for on-skin or implantable uses.[32,33]

Finally, the activation energy E_A (calculated using Equation (2) in Experimental Methods at a temperature interval from 290 to 305 K, before mobility-related changes come into play) of OSGTs (Figure 2h) provides information on the behavior of the barrier during operation. Indeed, we see that the height of the barrier in the Cu-contact devices is lower than that in the Ni-contact devices, despite non-uniformity. The barrier height of the Ni-contact OSGT with $d = 60$ µm stands out, as even though it is higher, it is much more easily pulled down by V_{GS}. This feature, which is assured in bulk-unipolar heterostructure SGTs,[34] may be useful if a certain temperature dependence of the on-state drain current is sought.

2.3. Operation as Phototransistors

The transfer characteristics of transistors with Au (**Figure 3**a), Cu (Figure 3b), and Ni (Figure 3c) contacts reveal that the Cu-contact DNTT OPSGTs are indeed highly V_{th}-stable when exposed to light with an incident power ($P_{incident}$) of 819 µW, which is in the ballpark of home living/dining room illumination.[35] This would translate to improved device-to-device uniformity, which is essential for yield improvement in manufacturing technologies using low-cost high-throughput methods, such as roll-to-roll processes,[36] which would be required to make the anticipated billions of disposable smart tattoos or bio-sensors. In a previous study, Milvich et al.[7] attributed the observed light-induced V_{th} shift to an additional charge sheet forming either at the Al_2O_3 interface, following tunneling of electrons through the 1.7 nm SAM layer, or at the SAM/DNTT interface at grain boundaries, and other defects. As mentioned earlier, the quasi-Fermi level of SGTs resides in the mid-gap both in the on-state and in the off-state. As such, subthreshold conduction is relatively unaffected by light-induced charge-trapping.

It is interesting to note that the Ni-contact device with $d = 10$ µm, shows a very strong reaction to light, but with a non-ideal off-state. The irregularity is likely to be isolated to this device, as SGTs, and by extension OSGTs, should have improved off-state operation over conventional devices.[27,37] In fact, the majority of Cu-contact and Ni-contact devices do show lower off-state drain currents than the Au-contact devices, and the off-state drain currents could be even lower, however, the noise-floor of the SMU limits the ability to detect these levels. That being said, further investigation might be warranted for short-channel devices.

The output characteristics show current crowding in the Au-contact device with $d = 60$ µm when exposed to light (Figure 3d). Its saturation behavior at $V_{DSAT2} = V_{GS}-V_{th}$ is the same, as expected. The saturation behavior is also the same in the device with Cu contacts of the same geometry (Figure 3e). The Ni-contact device (Figure 3f), on the other hand, demonstrates a change in saturation, whereby in dark conditions, it saturates at V_{DSAT1}, but upon light exposure saturates close to V_{DSAT2}, a situation attributed to a combination of photogeneration within the source-drain gap and the increase in charge-carrier concentration at the semiconductor-insulator interface at the edge of the source, which makes full depletion of the semiconductor layer mode difficult. NDR is also no longer present, which might offer insight into the origins of NDR, as a topic for a future study. This change in output conductance,for example, for drain-source voltage in the range of 5–10 V, could prove a useful path for light detection by means of amplitude or frequency modulation in circuits comprising OPSGTs as active loads.

The photo-to-dark current ratio (PDCR) of devices with various d, operating at $V_{GS} = 1$ V, shows that V_{th} stability is highly critical for optimum performance. Even though devices with Au (**Figure 4**a) and Cu contacts (Figure 4b) both exhibit a PCDR of $\approx 10^6$, the Cu-contact transistors are indeed the optimal case in terms of uniformity, with the Ni-contact OPSGTs (Figure 4c) having only slightly lower PDCR.

Even though the Cu-contact devices outperform both the Au-contact and the Ni-contact devices, there are benefits for using each architecture. In response to various values of $P_{incident}$, the Au-contact devices (Figure 4d) are more sensitive to low intensities of light. At higher $P_{incident}$, current crowding is normally witnessed in the output characteristics, yet here we see a slight decrease. This is likely due to the lifetime of the devices after being exposed to long periods in ambient air during measurement.

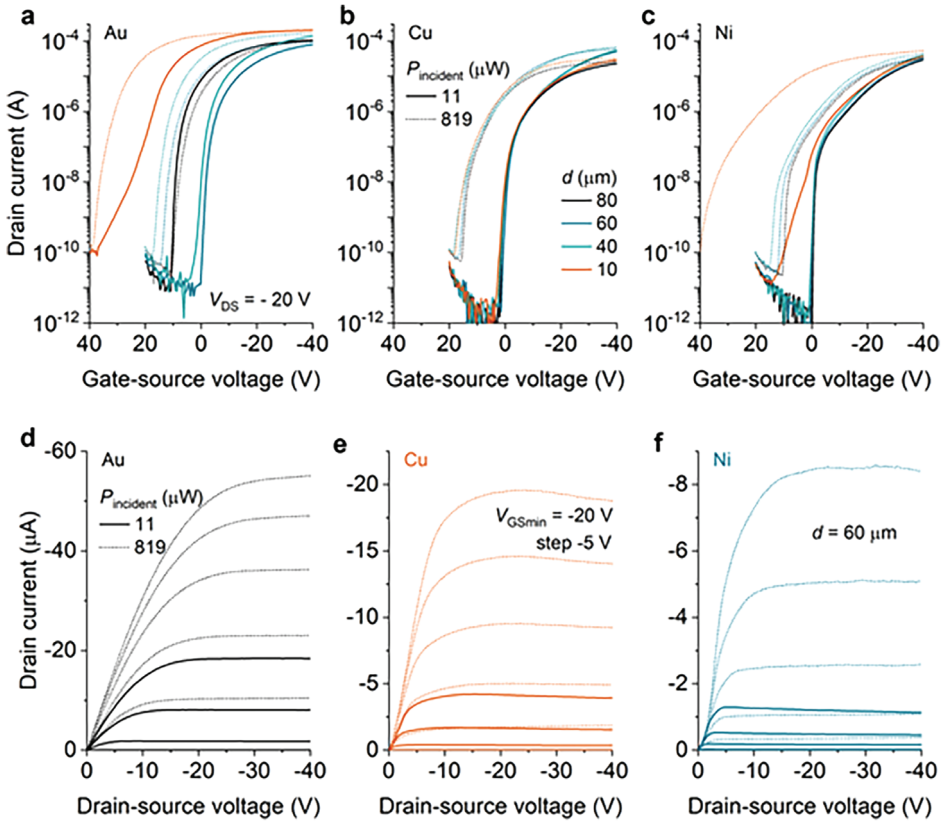

Figure 3. Transfer characteristics in dark and light conditions for transistors with a) Au, b) Cu, and c) Ni contacts. Cu OSGTs show the greatest V_{th} stability and d independence. Ni devices show wide dynamic range of on-current above threshold in the dark condition. Output characteristics for d) Au, e) Cu, and f) Ni OSGTs in dark and light conditions, demonstrating that all devices produce increased current under illumination, however, saturation behavior only changes qualitatively in the Ni devices, due to higher drain-source voltage V_{DS} required to pinch-off at the source when illuminated.

Previous DNTT OSGTs demonstrated greater stability in ambient air over Au OTFTs.[14] The Cu-contact OPSGTs (Figure 4e), though, have a strong, linear relationship between the drain current and $P_{incident}$, making them ideal as simple transducers. The Ni-contact OPSGTs (Figure 4f) are clearly more sensitive to a wider range of illumination, which is enabled by the ease with which the barrier is pulled down during operation (Figure 2h). One could envisage a simple application in which transistors with different contacts would overlap their response characteristics for an accurate and facile coverage of a wide dynamic range of incident light.

Aside from PDCR, important figures of merit for photodetectors are responsivity and detectivity.[38] Since a broad-spectrum source is utilized here, reporting detectivity would not give meaningful information. Responsivity calculations for $P_{incident}$ = 819 μW, yield values in the order of 5.5, 2, and 0.8×10^6 AW^{-1} for the transistors in Figure 3, with Au, Cu and Ni contacts, respectively, and d = 60 μm. This performance is competitive with recently-reported GeS source-gated phototransistors,[39] considering that, here, only a small fraction of the incident power is in fact within the absorption spectrum.

Finally, all transistors demonstrate a high PDCR even for V_{GS} = 0 V (Figure 4g). This greatly simplifies the realization of detector circuits, effectively operating the transistor as a two-terminal device. In this context, the Ni-contact OPSGT holds an additional performance advantage over the other transistors considered, namely its low V_{DSAT} under illumination. This is important for the development of wearable applications, as supply rails are likely to be regulated to 3.3 V or fed directly from a 3.7 to 4.3 V lithium secondary battery in many internet of things (IoT) applications.[32] While the PDCR here is lower than the value of 10^9 reported by Milvich et al.,[7] the integration time here was much shorter. It would be interesting, as a next step, to see how Cu and Ni OPSGTs compare to other DNTT OPTs[6,15] in response to illumination at the peak wavelength of 450 nm.

3. Conclusions and Outlook

This study has demonstrated the versatile nature of organic source-gated phototransistors, whereby the nature of the barrier determines the transistors' transconductance and hence their photosensitivity with respect to the incident light power. The linear dependence of the drain current on incident light power in the Cu-contact devices, as well as the exponential dependence of the behavior of the Ni-contact devices at higher incident powers, complements the low-light-sensing capability of the Au-contact phototransistors. Future designs could take advantage of all device architectures presented here, allowing for easy-to-fabricate and low-cost optical sensing applications.

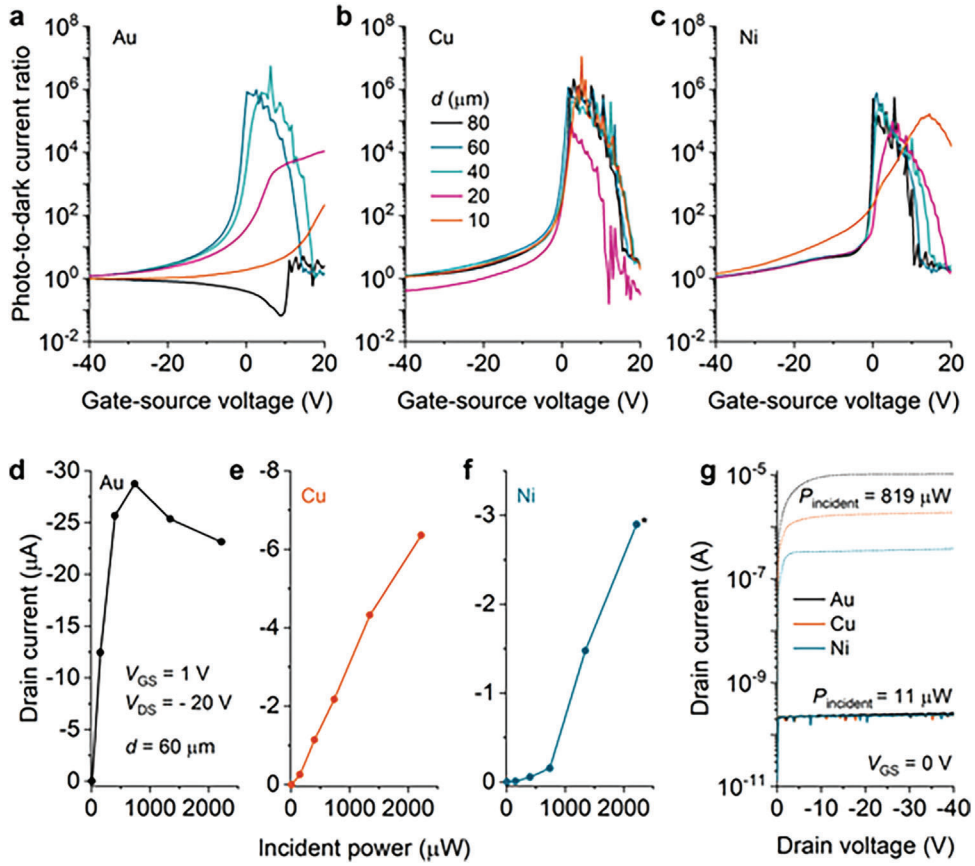

Figure 4. Photo-to-dark current ratio (PDCR) for a) Au, b) Cu, and c) Ni phototransistors. Specifically for the Cu-contact transistor, stable V_{th} operation translates to stability in PDCR. Varying incident light power in the d) Au device demonstrates sensitivity to the lower range, while the e) Cu device shows a strong linear trend across all intensities, and the f) Ni device is sensitive to the higher range. The data point with the asterisk was measured 1 week later. g) The output characteristics show low-voltage saturation in the Ni device is retained at $V_{GS} = 0$, which is beneficial for operating in saturation while powered directly, for example, from a Li-based battery.

4. Experimental Section

Device Fabrication: Organic thin-film transistors were fabricated in a bottom-gate, top-contact (BGTC) architecture, with different metal source/drain contacts: Au, Cu (Figure 1a), and Ni (Figure 1b). The substrate used was heavily *p*-type-doped Si with 100 nm thermally grown SiO_2. The doped Si is used as a global back-gate electrode and the SiO_2 forms part of the gate insulator stack, along with: 8 nm Al_2O_3, which was deposited using atomic layer deposition (ALD) at a temperature of 250 °C; and a *n*-tetradecylphosphonic acid ($C_{14}H_{29}PO(OH)_2$; PCI Synthesis, Newburyport, MA, USA)[40] self-assembled monolayer (SAM), which was deposited by immersing the samples into a 2-propanol and phosphonic acid solution. Next, the active layer was deposited via thermal sublimation of 25 nm dinaphtho[2,3-b:2′,3′-f]thieno[3,2-b]thiophene (DNTT, Figure 1c, Sigma Aldrich)[12] in vacuum at a rate of 0.3 $Å s^{-1}$ (sample temperature maintained at 60 °C). Source and drain contact electrodes were deposited through a shadow mask by thermal evaporation at a rate of 0.3 $Å s^{-1}$. Device features include width $W = 200$ μm and various channel lengths L. In SGTs, the geometrical channel was referred to as the source-drain separation d (Figure 1b,d), as during device operation, the nature of depletion at the source was different from conventional TFTs,[13] hence the alternative nomenclature. SGTs also differed in that the source-gate overlap S (Figure 1b) was a design parameter,[17] as the contact controls charge injection processes.[9] Here, the source-gate overlap was $S = 200$ μm (Figure 1d) by design, however during probing was shortened, due to placement of the probe tips. Probe placement was kept to a distance where $S > 100$ μm. This helped to ensure that measurements were taken in a region where the resistance was too great to contribute to any additional current, which was called as S_{SAT}.[17] Individual transistors were isolated by scoring the DNTT around the contacts, in order to reduce gate leakage currents. The gate was contacted by exposing the Si under the gate insulator layers with a diamond scribe.

Device and Incident Light Characterization: Transistors were characterized using a Wentworth probe station and a Keysight B2902A source/measure unit, driven by QuickIV software. Unless otherwise stated, the measurements were conducted at ambient temperature $T = 16.7$ °C (measured with a Hanna HI 8757 K-Type thermocouple with an accuracy of +/−0.5%). The HC250 temperature controller was connected to the chuck on the probe station. During temperature measurements, the hot-chuck controller was varied from $T = 25$ to 65 °C in 5 °C steps. Readings from the Hanna thermocouple connected to the substrate surface using thermal paste had been converted to Kelvin. The thermocouple readings were consistently 1.5 °C below the chuck controller setting.

Activation energy E_A was calculated using:

$$E_A = -\frac{\partial (\ln I_D)}{\partial \left(\frac{1}{kT}\right)} \quad (2)$$

where I_D was the drain current, and k was Boltzmann's constant. Threshold voltage V_{th} was extracted by taking the square root of I_D and fitting a straight line to intercept gate-source voltage axis.[41] Strictly speaking, V_{th} in SGTs was not the same as FETs, as explained in,[14] however this method was useful for comparison between devices.

For optical measurements, a Schott KL1500 LCD fiber optic cold light illuminator was used to expose devices to various light conditions (see Figure 1e for averaged spectral response). The distance from the fiber optic light source to the sample was ≈5 cm (Figure 1e). The incident light was characterized with an Ocean Optics USB4000 spectrometer and a Gentec XLP12 spectral power meter, which comprised a thermal head with 1.2 cm^2 capture area. Thus, measurements reported here as μW, correspond to μW(1.2)cm^{-2}. Transfer and output characteristics were measured in dark and light conditions, where the dark condition incident power $P_{incident} = 11$ μW, and the light condition was $P_{incident} = 819$ μW, including contribution from ambient room light (Figure 1f). Following characterization of devices with various d (or L), a device with $d = 60$ μm was chosen for each of the metal contacts (Au, Cu, and Ni) and measured at different $P_{incident}$ by varying the aperture setting (without additional ambient room light), which doubled the light intensity with each setting from A to E (Figure 1f). The $P_{incident} = 11$ μW dark condition was not in complete blackout, as some sources of light from equipment and the laboratory door was present, but any contributions would be negligible and were not visibly affecting measurements during characterization.

Acknowledgements

R.A.S. acknowledges EPSRC support via grant EP/V002759/1.

Conflict of Interest

The authors declare no conflict of interest.

Data Availability Statement

The data that support the findings of this study are available from the corresponding author upon reasonable request.

Keywords

optical sensing, organic thin-film transistors, phototransistors, Schottky contacts, source-gated transistors, stability

Received: August 9, 2023
Revised: September 12, 2023
Published online: October 13, 2023

[1] K. J. Baeg, M. Binda, D. Natali, M. Caironi, Y. Y. Noh, *Adv. Mater.* **2013**, *25*, 4267.
[2] S. R. Forrest, *Front. Opt. Photonics* **2021**, *10*, 31.
[3] W. Deng, Y. Lv, X. Ruan, X. Zhang, R. Jia, Y. Yu, Z. Liu, D. Wu, X. Zhang, J. Jie, *Laser Photonics Rev.* **2022**, *16*, 2200283.
[4] S. Hong, S. H. Choi, J. Park, H. Yoo, J. Y. Oh, E. Hwang, D. H. Yoon, S. Kim, *ACS Nano* **2020**, *14*, 9796.
[5] H. Zhang, X. Ju, D. Chi, L. Feng, Z. Liu, K. Yew, M. Zhu, T. Li, R. Wei, S. Wang, L. Sun, Z. Wang, Y. Wu, *Appl. Mater. Today* **2023**, *33*, 101885.
[6] M. Scagliotti, A. Valletta, S. Calvi, L. Mariucci, M. Rapisarda, *IEEE Sens. Lett.* **2023**, *7*, 1.
[7] J. Milvich, T. Zaki, M. Aghamohammadi, R. Rödel, U. Kraft, H. Klauk, J. N. Burghartz, *Org. Electron.* **2015**, *20*, 63.
[8] J. M. Shannon, E. G. Gerstner, *IEEE Electron Device Lett.* **2003**, *24*, 405.
[9] J. M. Shannon, R. A. Sporea, S. Georgakopoulos, M. Shkunov, S. R. P. Silva, *IEEE Trans. Electron Devices* **2013**, *60*, 2444.
[10] A. Valletta, L. Mariucci, M. Rapisarda, G. Fortunato, *J. Appl. Phys.* **2013**, *114*, 064501.
[11] G. Wang, X. Zhuang, W. Huang, J. Yu, H. Zhang, A. Facchetti, T. J. Marks, *Adv. Sci.* **2021**, *8*, 2101473.
[12] U. Kraft, K. Takimiya, M. J. Kang, R. Rödel, F. Letzkus, J. N. Burghartz, E. Weber, H. Klauk, *Org. Electron.* **2016**, *35*, 33.
[13] E. Bestelink, U. Zschieschang, I. Bandara R M, H. Klauk, R. A. Sporea, *Adv. Electron. Mater.* **2021**, *8*, 2101101.
[14] E. Bestelink, H. Teng, U. Zschieschang, H. Klauk, R. A. Sporea, *Adv. Electron. Mater.* **2023**, *9*, 2201163.
[15] F. Yu, S. Wu, X. Wang, G. Zhang, H. Lu, L. Qiu, *RSC Adv.* **2017**, *7*, 11572.
[16] E. Bestelink, O. de Sagazan, L. Motte, B. Schultes, S. R. P. Silva, R. A. Sporea, *Adv. Intell. Syst.* **2020**, *3*, 2000199.
[17] R. A. Sporea, S. R. P. Silva, in *2017 Int. Semiconductor Conf. (CAS)*, IEEE, Piscataway, NJ **2017**, pp. 155–158.
[18] S. D. Brotherton, *Introduction to Thin Film Transistors: Physics and Technology of TFTs*, Springer International Publishing, Switzerland **2013**.
[19] R. A. Sporea, M. J. Trainor, N. D. Young, J. M. Shannon, S. R. P. Silva, *IEEE Trans. Electron Devices* **2010**, *57*, 2434.
[20] J. Zhang, J. Wilson, G. Auton, Y. Wang, M. Xu, Q. Xin, A. Song, *Proc. Natl. Acad. Sci. U. S. A.* **2019**, *116*, 4843.
[21] S. Mansouri, A. Jouili, L. El Mir, A. A. Al-Ghamdi, F. Yakuphanoglu, *Synth. Met.* **2015**, *207*, 1.
[22] M. Mahdouani, W. Boukhili, R. Bourguiga, *Mater. Today Commun.* **2017**, *13*, 367.
[23] E. Bestelink, P. Sihapitak, U. Zschieschang, L. Askew, J. M. Shannon, J. P. Bermundo, Y. Uraoka, H. Klauk, R. A. Sporea, *J. Mater. Chem. C* **2023**, *11*, 11688.
[24] X. Zhuang, J. Kim, W. Huang, Y. Chen, G. Wang, J. Chen, Y. Yao, Z. Wang, F. Liu, J. Yu, Y. Cheng, Z. Yang, L. J. Lauhon, T. J. Marks, A. Facchetti, *Proc. Natl. Acad. Sci. U. S. A.* **2023**, *120*, e2216672120.
[25] J. M. Shannon, E. G. Gerstner, *Solid-State Electron.* **2004**, *48*, 1155.
[26] R. A. Sporea, M. J. Trainor, N. D. Young, J. M. Shannon, S. R. P. Silva, *Sci. Rep.* **2014**, *4*, 4295.
[27] R. A. Sporea, M. J. Trainor, N. D. Young, X. Guo, J. M. Shannon, S. R. P. Silva, *Solid-State. Electron.* **2011**, *65–66*, 246.
[28] H. Chen, W. Zhang, M. Li, G. He, X. Guo, *Chem. Rev.* **2020**, *120*, 2879.
[29] M. Chen, B. Peng, R. A. Sporea, V. Podzorov, P. K. L. Chan, *Small Sci.* **2022**, *2*, 2100115.
[30] J. M. Shannon, *Appl. Phys. Lett.* **2004**, *85*, 326.
[31] R. A. Sporea, M. Overy, J. M. Shannon, S. R. P. Silva, *J. Appl. Phys.* **2015**, *117*, 184502.
[32] E. Bestelink, H.-J. Teng, R. A. Sporea, *IEEE Trans. Electron Devices* **2021**, *68*, 4962.
[33] S. Jeon, S. C. Lim, T. Q. Trung, M. Jung, N. E. Lee, *Proc. IEEE* **2019**, *107*, 2065.
[34] R. A. Sporea, K. D. G. I. Jayawardena, M. Constantinou, M. Ritchie, A. Brewin, W. Wright, S. R. P. Silva, *ECS Trans.* **2016**, *75*, 61.
[35] *Energy Standard for Buildings Except Low-Rise Residential Buildings*, ANSI, Washington, DC, USA **2012**.
[36] A. F. Paterson, T. D. Anthopoulos, *Nat. Commun.* **2018**, *9*, 5264.
[37] E. Bestelink, T. Landers, R. A. Sporea, *Appl. Phys. Lett.* **2019**, *114*, 182103.
[38] Z. Sa, F. Liu, X. Zhuang, Y. Yin, Z. Lv, M. Wang, J. Zhang, K. Song, F. Chen, Z.-X. Yang, *Adv. Funct. Mater.* **2023**, *33*, 2304064.
[39] M. Wang, X. Zhuang, F. Liu, Y. Chen, Z. Sa, Y. Yin, Z. Lv, H. Wei, K. Song, B. Cao, Z. X. Yang, *Nano Lett.* **2022**, *22*, 9707.
[40] S. Bisoyi, R. Rödel, U. Zschieschang, M. J. Kang, K. Takimiya, H. Klauk, S. P. Tiwari, *Semicond. Sci. Technol.* **2016**, *31*, 025011.
[41] E. G. Bittle, J. I. Basham, T. N. Jackson, O. D. Jurchescu, D. J. Gundlach, *Nat. Commun.* **2016**, *7*, 10908.